A Correction to the Baroclinic Pressure Gradient Term in the Princeton Ocean Model

ROBIN ROBERTSON,* LAURIE PADMAN,+ AND MURRAY D. LEVINE

College of Oceanic and Atmospheric Sciences, Oregon State University, Corvallis, Oregon

(Manuscript received 26 May 2000, in final form 7 December 2000)

ABSTRACT

An error in the calculation of the baroclinic pressure gradient term in the Princeton Ocean Model (POM) was identified while modeling the M_2 tidal current near its critical latitude in the southern Weddell Sea. The error arises from the present calculation of density, which involves the subtraction of a background density profile from the density field calculated at each internal time step. The small displacement of sigma surface depths relative to the surface, as surface elevation changes, causes a slight error in the calculation of the vertical and horizontal gradients of potential density. The error is largest at the seabed over rapidly changing bathymetry such as the continental slope. The baroclinic pressure gradient error is typically much smaller than the Coriolis term in the momentum equations and, therefore, usually unimportant. Close to the critical latitude, however, near-resonance between the error and Coriolis terms can cause an energetic and spatially complex spurious inertial mode to develop. The error is significant when modeling tides near their critical latitudes, and will contribute to the error in the baroclinic pressure gradient in other simulations. Two methods were suggested for fixing this problem. The preferred method was tested by applying the new form of POM to the southern Weddell Sea. The new results are consistent with both current meter data and predictions of linear internal wave theory.

1. Introduction

Various numerical errors arising from the baroclinic pressure gradient term in sigma coordinate models have been previously discussed (e.g., Kleim and Pietrzak 1999; Mellor et al. 1994, 1998). Kleim and Pietrzak (1999) evaluate the baroclinic pressure gradient error in sigma coordinate models, considering specifically the Princeton Ocean Model (POM) (described in Blumberg and Mellor 1987; Mellor 1998; Robertson 1999). For cases where the ocean surface is treated as a rigid lid, they state that ''The pressure gradient error arises owing to truncation error in the discretization'' of the baroclinic pressure gradient equation. The standard version of POM, however, uses a free surface boundary condition, which leads to an additional source of error in the baroclinic pressure gradient term. This error, which is the topic of this paper, can produce a spatially complex inertial oscillation and was identified while modeling the vertical structure of M_2 tidal currents in the Weddell Sea (Robertson 1999). Baroclinic tides are generally understood to be generated through interactions of the barotropic tide and the continental slope. The continental slope in this region is close to the M_2 critical latitude ψ_{crit}, which is the latitude (ψ) at which the tidal frequency ω_{tide} equals the inertial frequency f. This newly identified error is associated with the incorrect treatment of time-varying surface elevation (η) in the calculation of in situ density. The error term is orders of magnitude smaller than the dominant term (Coriolis) in the momentum equations. Close to ψ_{crit}, however, the error can resonantly force an inertial oscillation that can grow to exceed the original energy in the barotropic tide.

First, the error and its source are described (section 2). Details of POM appear elsewhere (e.g., Mellor 1998) and so are not repeated here. The topographic, hydrographic, and boundary conditions used are fully described in Robertson (1999) and Robertson (2001a,b). The modifications that were made to POM to eliminate the error are described in section 3, and comparisons of model results before and after the modification are presented in section 4.

2. The problem

The research that led to identification of this error was a study of the depth variability of M_2 tidal currents in the Weddell Sea (Robertson 1999), using a quasi-two-dimensional ''transect'' version of POM in a manner similar to that of Holloway (1996). The model was applied to a transect across the continental shelf and

* Current affiliation: Alfred-Wegener-Institut, Bremerhaven, Germany.

+ Current affiliation: Earth and Space Research, Seattle, Washington.

Corresponding author address: Dr. Robin Robertson, Alfred-Wegener-Institut, Postfach 12 01 61, D-27515 Bremerhaven, Germany.
E-mail: rrobertson@ldeo.columbia.edu or rrobertson@awi-bremerhaven.de

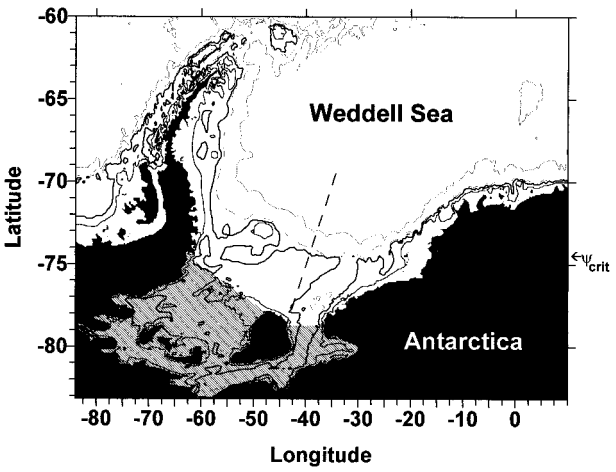

FIG. 1. The water column thickness for the Weddell Sea, contoured at 200, 500 (thick line), 1000 (dashed line), and 3000 m. The Filchner–Ronne Ice Shelf area is indicated by hatching. The location of the transect used for the model domain is shown as a dashed line.

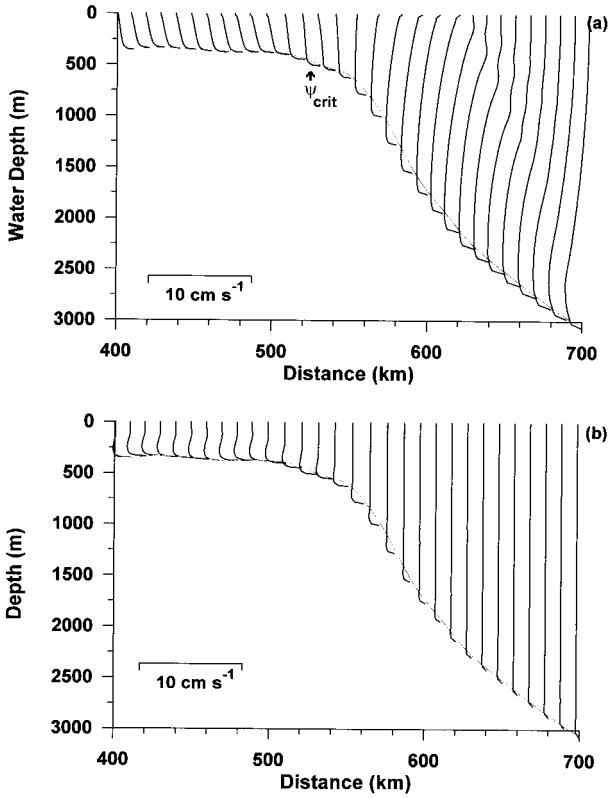

FIG. 2. Cross-slope velocity profiles at a time near the peak onshore flow over the continental slope from simulations using the original version of POM without stratification both (a) with and (b) without the critical latitude in the domain. The location of ψ_{crit} is indicated in (a).

slope (Fig. 1), where $\psi_{crit}(M_2)$ ($\approx$74°28′S) is located near the shelf break. Wave dynamics are modified in the vicinity of ψ_{crit}, since it is the poleward limit for both internal (Kundu 1990) and Poincaré wave propagation (Middleton and Denniss 1993). Near ψ_{crit}, inertial oscillations can be induced by the tide, and the momentum boundary layer for the tidal constituent can become thick and complex, even without stratification effects (Foldvik et al. 1990; Furevik and Foldvik 1996). Boundary effects are seen in both mooring data and analytical models, that is, they are not simply numerical model artifacts of the type reported herein.

As part of the diagnosis of suspected errors in the baroclinic version of POM, the model was applied to a homogeneous ocean (uniform potential temperature, θ, and salinity, S). The model was forced by specifying the M_2 barotropic tidal elevations at the northern and southern ocean boundaries. In this configuration, an energetic depth-dependent oscillation developed over the continental slope. Both the magnitude and phase of the oscillation, which was initially interpreted as variation at the M_2 frequency, had a complex cross-slope structure (Figs. 2a and 3a). [For Fig. 3a, the major axes of the tidal ellipses were determined using Foreman's routines (Foreman 1978) applied only to the last 2 days of the model run.] When POM was used with the same topography and forcing but with ψ_{crit} to the south of the domain, the cross-slope velocity field was nearly constant with depth except, as expected, for the benthic boundary layer (Fig. 2b).

Is this depth-dependent oscillation in the critical-latitude case real? Velocity profiles with such a strong benthic signal, greater than 10 cm s^{-1} in 1000-m water depth, at the M_2 frequency have not been observed in current meter measurements made in this region (Middleton and Foster 1977; Middleton et al. 1982; Foldvik et al. 1990; Woodgate et al. 1998). These observations, combined with the strong dependence of the amplitude of the final velocity field on model run length, persuaded us that the oscillation was somehow an artifact of the numerical scheme.

What then, is the apparently numerical cause of these oscillations? This problem was approached by examining the "baroclinic mode" momentum equation for the cross-slope depth-dependent velocity, V, expressed in sigma coordinates (x, y, σ). Here, x and y are the alongslope and cross-slope horizontal distances, respectively, and σ is the fractional vertical distance in the water column from the seabed to the free surface ($-1 \le \sigma \le 0$):

$$\frac{\partial VD}{\partial t} + \frac{\partial UVD}{\partial x} + \frac{\partial VVD}{\partial y} + \frac{\partial VW'}{\partial \sigma} + fUD + gD\frac{\partial \eta}{\partial y} + gD^2 \int_{\sigma}^{0} \left[\frac{\partial \rho'}{\partial y} - \frac{\sigma'}{D}\frac{\partial D}{\partial y}\frac{\partial \rho'}{\partial \sigma'}\right] d\sigma' = \frac{\partial}{\partial \sigma}\left[\frac{K_M}{D}\frac{\partial V}{\partial \sigma}\right] + \frac{\partial}{\partial x}\left[DA_M\left(\frac{\partial U}{\partial y} + \frac{\partial V}{\partial x}\right)\right] + \frac{\partial}{\partial y}\left[2DA_M\frac{\partial V}{\partial y}\right]. \quad (1)$$

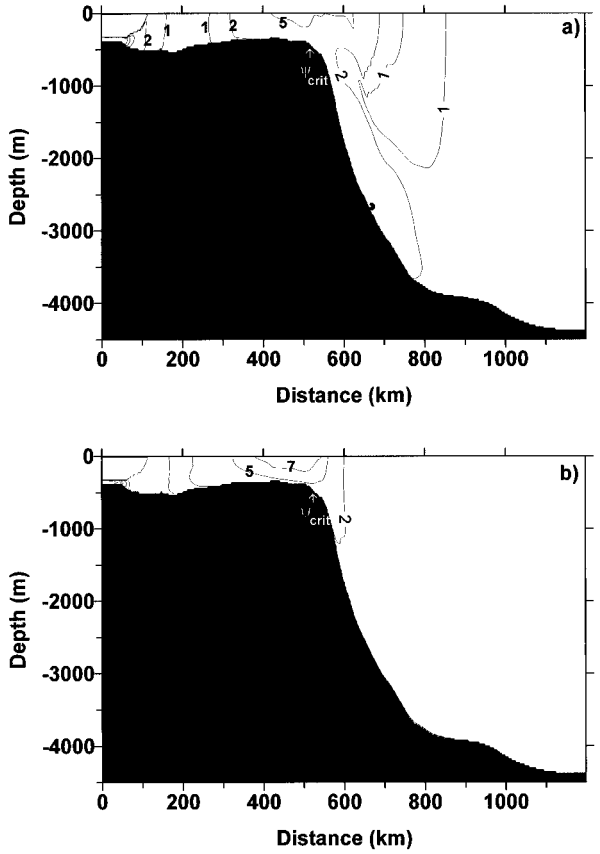

FIG. 3. The major axes of the tidal ellipses of the depth-dependent velocities (cm s^{-1}) from simulations with the critical latitude in the domain and a homogeneous ocean from (a) the original version of POM and (b) the modified version of POM.

In (1), U is the alongslope depth-dependent velocity, W' is the vertical velocity, η is the surface elevation, and t is time. Depth $D = H + \eta$ is the water column thickness, where H is the water depth for the system at rest. The perturbation density ρ' will be described more fully later. Other variables are the Coriolis parameter f, gravitational acceleration g (9.8 m s^{-2}), horizontal viscosity coefficient A_M (m^2 s^{-1}), and the vertical viscosity coefficient K_M (m^2 s^{-1}). The momentum balance consists of terms for [in order of their appearance in (1)] acceleration, advection in the alongslope, cross-slope, and vertical directions, Coriolis force, surface elevation pressure gradient, baroclinic pressure gradient (BPG), vertical diffusion, and horizontal diffusion, in that order. Only the Coriolis force, BPG, and diffusion terms varied with depth in the POM simulation for a homogeneous ocean. The BPG in this case, however, should be zero, indicating that the BPG is a probable source of error.

Time series (not shown) of the various terms in (1) for the homogeneous case and for various (y, σ) coordinates, show that the BPG is at least 1–2 orders of magnitude smaller than the Coriolis term but varies significantly with y and σ, being greatest at the seabed over the continental slope. The effect of this error acceleration term in the momentum equations would normally be small since the term itself is small relative to other terms (in this case, the Coriolis term). When the frequency of the error BPG is close to f, however, near-resonant forcing may cause the growth of a significant inertial mode during a sufficiently long model run.

Plausible candidates for the specific feature of the BPG calculation that produces the error include truncation errors, C-grid errors, and a systematic numerical error in the calculation of $\partial p/\partial y$. Kleim and Pietrzak (1999) reported truncation errors in POM, which result from the differencing of two large nearly equal values used in the present BPG calculation. Due to the use of the sigma coordinate system, the BPG term in (1) is the difference of two terms:

$$\text{BPG} = gD^2 \int_{\sigma}^{0} \left[\frac{\partial \rho'}{\partial y} - \frac{\sigma'}{D} \frac{\partial D}{\partial y} \frac{\partial \rho'}{\partial \sigma'} \right] d\sigma'. \quad (2)$$

In (2), ρ' is the perturbation density defined by

$$\rho'(x, y, \sigma, t) = \rho(x, y, \sigma, t) - \rho_{\text{MEAN}}(x, y, \sigma). \quad (3)$$

In (3), ρ is the in situ density and ρ_{MEAN} is a horizontally averaged, time-independent initial in situ density field. To maximize numerical accuracy, ρ (and, thus, also ρ_{MEAN}), is normalized as

$$\rho = \frac{\rho_{P,\theta,S} - \rho_o}{1000}, \quad (4)$$

where $\rho'_{P,\theta,S}$ is the dimensional in situ density written as the sum of a function of θ and S plus a function of pressure, that is,

$$\rho_{P,\theta,S}(x, y, \sigma, t) = \rho_{\theta,S}[\theta(x, y, \sigma, t), S(x, y, \sigma, t)] + \rho_p(p/c^2). \quad (5)$$

In (4), ρ_o is a general mean density, which was set to 1025 (or 1000) in the original POM. In (5), c is the sound speed in meters per second, $\rho_{\theta,S}$ is the potential density, ρ_p is given by

$$\rho_p = 10^4 \frac{p}{c^2} \left(1 - 0.2 \frac{p}{c^2} \right), \quad (6)$$

and the hydrostatic pressure is approximated by

$$p(\sigma D) = -\rho_o g 10^{-4} D\sigma = -\rho_o g 10^{-4} (H + \eta)\sigma. \quad (7)$$

In (6) and (7), the factors 10^4 and 10^{-4} convert between pressures in Pascals and in decibars. The sound speed c is approximated by

$$c = 1449.1 + 0.00821p + 4.55\theta - 0.45\theta^2 + 1.34(S - 35). \quad (8)$$

Note that the constant in (8), 1449.1, is as in the original version of the POM code. This form of the equation follows Mellor (1991); however, the constant in (8) in Mellor (1991) is quoted as 1449.2, whereas it was 1449.1 in the original POM code, which was used. This difference is not expected to contribute significantly to this error. A full discussion of the errors in the equation of state is given in Mellor (1991).

The focus of this paper is the error that arises in the BPG because ρ_{MEAN} does not include the time-varying pressure due to $\eta(t)$ that is included in the calculation of p in (7). While this error is very small, it will be shown to be significant under certain conditions that are experienced in the real ocean. To demonstrate, consider the case of an unstratified ocean where θ and S are constant everywhere. For simplicity, it was further assumed that c^2 is constant. Then it was expected that $\rho' = 0$ everywhere. Indeed, the terms dependent on θ and S cancel, however,

$$\rho' = \frac{\rho_p[p(\sigma D)] - \rho_p[p(\sigma H)]}{\rho_o} \tag{9}$$

since the depth at which the pressure is calculated is slightly different in ρ and ρ_{MEAN} by $\sigma\eta = \sigma(D - H)$ meters. Note that ρ_o here represents the 1000 in (4). Now, defining two constants, $\alpha = gc^{-2}$ and $\beta = 2 \times 10^{-5}\rho_o g^2 c^{-4}$, ρ' becomes

$$\rho' = -\alpha\sigma\eta - \beta\sigma^2(D^2 - H^2). \tag{10}$$

Defining the integrand in (2) to be BC, it became

$$\text{BC} = -\alpha\sigma\frac{\partial\eta}{\partial y} - 2\beta\sigma^2\left(D\frac{\partial D}{\partial y} - H\frac{\partial H}{\partial y}\right) - \frac{\sigma}{D}\frac{\partial D}{\partial y}[\alpha\eta - 2\beta\sigma(D^2 - H^2)]. \tag{11}$$

Equation (11), after some arithmetic, reduces to

$$\text{BC} = \left[\frac{-\alpha\sigma}{D} - 2\beta\sigma^2\frac{H}{D}\right]\left[H\frac{\partial\eta}{\partial y} - \eta\frac{\partial H}{\partial y}\right]. \tag{12}$$

In (12), the second half of the first term is much smaller than the first half, due to the c^{-4} factor; furthermore, it is expected that $\eta\partial H/\partial y$ will exceed $H\partial\eta/\partial y$ over the continental slope, since the topographic scales of variability are generally smaller than the wavelength of the barotropic tide. Thus, neglecting $H\partial\eta/\partial y$ and the second half of the first term, it was found that BC $\propto \eta\sigma\partial H/\partial y$. Since the error BPG (denoted $\text{BPG}_{\text{error}}$) is the downward integral (from the sea surface) of BC, it is given to leading order by

$$\text{BPG}_{\text{error}} \propto \eta\sigma^2\partial H/\partial y. \tag{13}$$

As expected from the model simulations with the uncorrected version of POM, (13) predicts that the strongest error forcing is at the seabed over steep topography. The value of $\text{BPG}_{\text{error}}$ is proportional to η so that a rigid lid upper boundary condition, as in the cases studied by Kleim and Pietrzak (1999), removes this particular source of error. The exact $\text{BPG}_{\text{error}}$ in POM as determined on the C grid is

$$\text{BPG}_{\text{error}} = \int_{\sigma}^{0} \frac{-g(\sigma_k + \sigma_{k+1})}{2c^2\Delta y}\left[(\eta_j - \eta_{j+1}) - \frac{(D_j - D_{j+1})(\eta_j + \eta_{j+1})}{(D_j + D_{j+1})}\right] - \frac{2\times 10^{-5}\rho_o g^2(2H_j\eta_j + \eta_j^2 - 2H_{j+1}\eta_{j+1} - \eta_{j+1}^2)}{2c^4\Delta y}\left[(\sigma_k^2 - \sigma_{k+1}^2) - \frac{(\sigma_k + \sigma_{k+1})^2(D_j - D_{j+1})}{2\Delta y(D_j + D_{j+1})}\right]\partial\sigma', \tag{14}$$

where j and k refer to the indices of the location being determined on the C grid in the cross-slope and vertical directions, respectively. Note that this term is of the same form as (12), however, with additional factors resulting from the use of a C grid.

Since the $\text{BPG}_{\text{error}}$ arises from η, which in this problem is primarily due to the barotropic tide that is forced by the northern and southern boundary conditions, it fluctuates at the tidal frequency. Near ψ_{crit}, $\text{BPG}_{\text{error}}$ is nearly resonant with f and can, therefore, induce inertial oscillations whose amplitudes increase as the model timestepping progresses. This occurs even though the magnitude of $\text{BPG}_{\text{error}}$ is much less than the Coriolis term.

Two factors act to ultimately stabilize the spurious inertial oscillations forced by $\text{BPG}_{\text{error}}$. First, as velocities increase, the increased benthic friction and momentum diffusion slow further growth of the inertial oscillations. The effect of friction was tested with a comparison of two homogeneous model runs, one using the values of K_M generated by POM, and the other with friction eliminated by removing the vertical diffusion of momentum. Without friction, it was expected that the magnitude U_e of the error inertial mode for fixed y would scale approximately with $\text{BPG}_{\text{error}}$ (13), that is, $U_e \propto \sigma^2$. In the high-viscosity run (Fig. 2a), vertical profiles of V over the slope are quite smooth, whereas, for the no friction case (not shown), U_e is much higher near the seabed, as expected from the quadratic dependence of $\text{BPG}_{\text{error}}$ on σ in (13). For this case, the spatial structure of U_e is qualitatively similar to that shown in the major axes for the stratified case (Fig. 6a). The difference between it and the stratified case (Fig. 6a) is a reduced

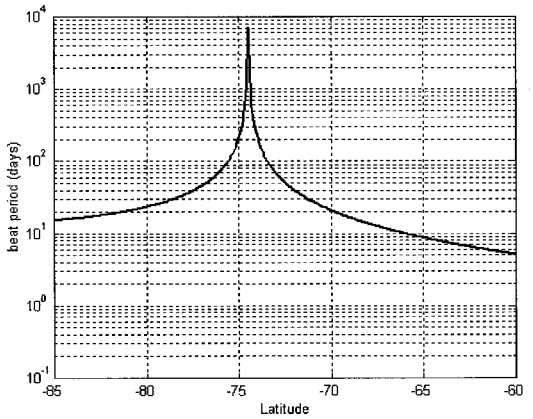

FIG. 4. The beat period (in days) between ω_{tide} and f as a function of latitude.

signal in the upper water column, which was due to the generation of a slight internal tidal signal in the stratified case. The effects of stratification are twofold: it may generate internal tides and it reduces the vertical viscosity coefficient, correspondingly adjusting the benthic boundary layer thickness.

Second, true resonance only exists precisely at ψ_{crit}, and even there, lateral diffusion of momentum due to horizontal viscosity will slowly detune the error inertial mode from the surface tidal forcing. Away from ψ_{crit}, the period during which $\text{BPG}_{\text{error}}$ will amplify the energy of the spurious inertial mode is some fraction of the ''beat period'' of the inertial mode and the tidal periodicity of $\eta(t)$. This beat period is simply $\tau_b = (\omega_{\text{tide}} - |f|)^{-1}$. Values of τ_b exceed 100 days for a band $\sim 3°$ wide around ψ_{crit} (Fig. 4). However, τ_b decreases to <10 days near $\psi = 66°$. Thus, at this latitude, during 5 days the phase between the forced inertial mode and the tidal forcing will shift by 180°, and the maximum amplification of the inertial mode by $\text{BPG}_{\text{error}}$ will be limited to the growth of the mode during a fraction of this time interval. A model run with a homogeneous ocean, and the domain shifted 10°N of ψ_{crit} so that the shelf break was near 65°S, supports this conclusion. In this case the effect of $\text{BPG}_{\text{error}}$ was negligible (Fig. 2b).

It is then seen how a complex structure can develop in a velocity field, when the velocity time series are analyzed for just the end of the model run. Although spectral analysis indicates that the variability occurred near the forced tidal frequency, it is unable to resolve the inertial and tidal frequencies, which results in the inertial oscillations being attributed to tidal motion. Depth dependence arises from the quadratic dependence of $\text{BPG}_{\text{error}}$ on depth (13). Cross-slope variation arises from changes in bottom slope $\partial H/\partial y$, the reduced efficiency of the resonance forcing as the meridional distance from ψ_{crit} increases, and because, at any given time, the phase relationship between the true tidal current and the forced inertial mode varies as a function of ψ. Additional modifications to the basic expectations

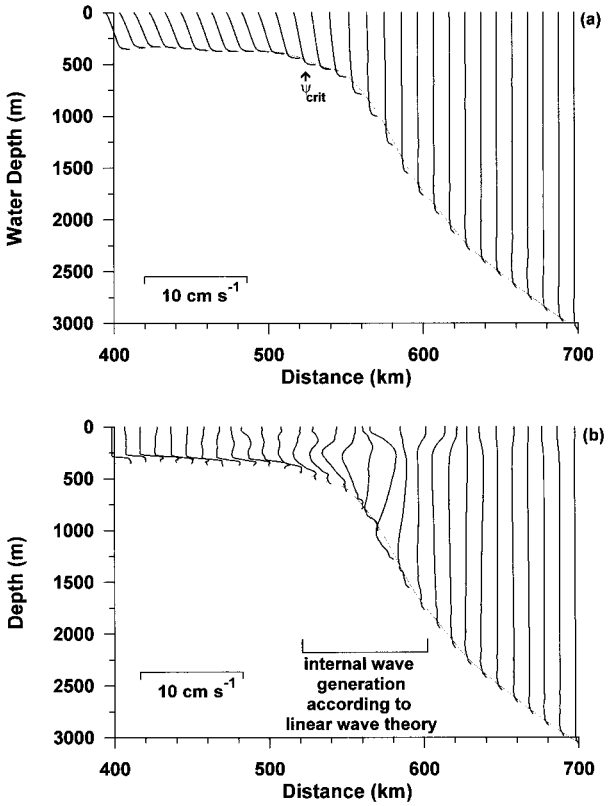

FIG. 5. Cross-slope velocity profiles at a time near the peak onshore flow over the continental slope, from simulations using the modified version of POM with the critical latitude in the domain and (a) without and (b) with stratification. The location of ψ_{crit} is indicated in (a). The region where linear internal wave theory predicts internal tides with this location of ψ_{crit} is indicated in (b).

based on (13) occur due to vertical and lateral viscosity, and ignoring $H\partial\eta/\partial y$ and the second term in (12). Since most previous internal tide investigations, such as those of Holloway (1996) on the Australian slope or Chen and Beardsley (1998) over Georges Bank, have not been located near ψ_{crit} for the tidal constituent being studied, these studies have not encountered this resonant error inertial response. This error also exists for cases with stronger stratification; however, the error is masked by the more intense internal tidal field, which develops with the stronger stratification.

3. Model modifications

The error in the BPG calculation arises through the incorrect handling of η in the calculation of perturbation density ρ' in (3). It was choosen to correct this error by using ρ directly, without subtracting ρ_{MEAN}. It is then possible to simplify further to $\rho = \rho_{\theta,S}$ (i.e., the potential density), since the contribution of $\rho_P[p(\sigma D)/c^2)]$ to *BC* is identically zero—that is, the pressure effects are exactly removed when the horizontal gradient of density is calculated for the BPG, leaving only the contribution from variations of θ and *S*. For the pressure effects to

exactly cancel, however, the pressure contributions of ρ_P must be determined at the location of the velocity point using derivatives and not calculated using differences on the C grid.

The primary justification for the present approach, subtracting ρ_{MEAN} from ρ, is to reduce the dynamic range of density in the calculations of the BPG and the buoyancy frequency N. The results, shown in the following section, indicate that the perturbation approach is not necessary, at least with weak stratification when working in double precision. It should be noted that ρ' in (3) is already very close to being a normalized potential density, since the removal of ρ_{MEAN} also removes the pressure contribution to in situ density ρ.

The cancellation of the pressure contribution can be easily seen if the normalized in situ density, ρ, is split into two portions—one from the potential temperature and salinity, ρ_N, and one from the pressure, ρ_P:

$$\rho(x, y, \sigma) = \rho_N[\theta(x, y, \sigma), S(x, y, \sigma)] + \rho_P[\sigma, D(x, y)]. \quad (16)$$

The BPG would then be determined from these two portions:

$$\text{BPG} = gD^2 \int_\sigma^0 \left[\frac{\partial \rho_N}{\partial y} + \frac{\partial \rho_P}{\partial y} - \frac{\sigma'}{D}\frac{\partial D}{\partial y}\frac{\partial \rho_N}{\partial \sigma'} - \frac{\sigma'}{D}\frac{\partial D}{\partial y}\frac{\partial \rho_P}{\partial \sigma'}\right] d\sigma'. \quad (17)$$

Furthermore, the pressure portion of density, ρ_P, is determined at the velocity point being calculated using the pressure relation:

$$\rho_P = -gc^{-2}D\sigma - (2 \times 10^{-5})\rho_o g^2 c^{-4} D^2 \sigma^2. \quad (18)$$

Taking the derivatives in the alongsigma and cross-sigma directions, while treating c as a constant, yields

$$\frac{\partial \rho_P}{\partial y} = -gc^{-2}\sigma\frac{\partial D}{\partial y} - (4 \times 10^{-5})\rho_o g^2 c^{-4} D\sigma^2 \frac{\partial D}{\partial y} \quad (19)$$

and

$$\frac{\partial \rho_P}{\partial \sigma} = -gc^{-2}D - (4 \times 10^{-5})\rho_o g^2 c^{-4} D^2 \sigma, \quad (20)$$

respectively.

Substituting these relations into BPG results in

$$\text{BPG} = gD^2 \int_\sigma^0 \left[\frac{\partial \rho_N}{\partial y} - gc^{-2}\sigma'\frac{\partial D}{\partial y} - (4 \times 10^{-5})\rho_o g^2 c^{-4} D\sigma'^2 \frac{\partial D}{\partial y} - \frac{\sigma'}{D}\frac{\partial D}{\partial y}\frac{\partial \rho_N}{\partial \sigma'} - \frac{\sigma'}{D}\frac{\partial D}{\partial y}[-gc^{-2}D - (4 \times 10^{-5})\rho_o g^2 c^{-4} D^2 \sigma']\right] d\sigma'. \quad (21)$$

After canceling terms, this reduces to

$$\text{BPG} = gD^2 \int_\sigma^0 \left[\frac{\partial \rho_N}{\partial y} - \frac{\sigma'}{D}\frac{\partial D}{\partial y}\frac{\partial \rho_N}{\partial \sigma'}\right] d\sigma'. \quad (22)$$

Since the gradients of the pressure portion cancel each other, only the potential temperature and salinity portion remains. It is easy to see that, with a homogeneous ocean, the gradients of the potential temperature and salinity portion would also be zero, as would BPG. The dependence of c in the along sigma and cross-sigma directions has been ignored in these derivatives. An error analysis has determined that it is negligible, $<10^{-10}$% given realistic values for the maximum gradients of θ, S, p, and H.

A second possible method for eliminating $\text{BPG}_{\text{error}}$ would be to set $\eta = 0$ in ρ_P used in the calculation of ρ, and then continue to use the perturbation density ρ' (3) with ρ_{MEAN} removed. If this is done, the pressure adjustments for the density and background density exactly cancel each other in (3) and the result is equivalent. However, this second solution method unnecessarily increases the number of computations performed and can also increase the truncation error.

To implement the above modification in POM, the pressure correction to density was removed in the density subroutine (DENS) as was the pressure correction to the Brunt–Väisälä frequency in the subroutine which determines the vertical viscosity (PROFQ). Additionally, since stratification is weak in the region of interest and the majority of the change in the background density is due to pressure, the normalized density, ρ, instead of the perturbation density, ρ', was used for determining

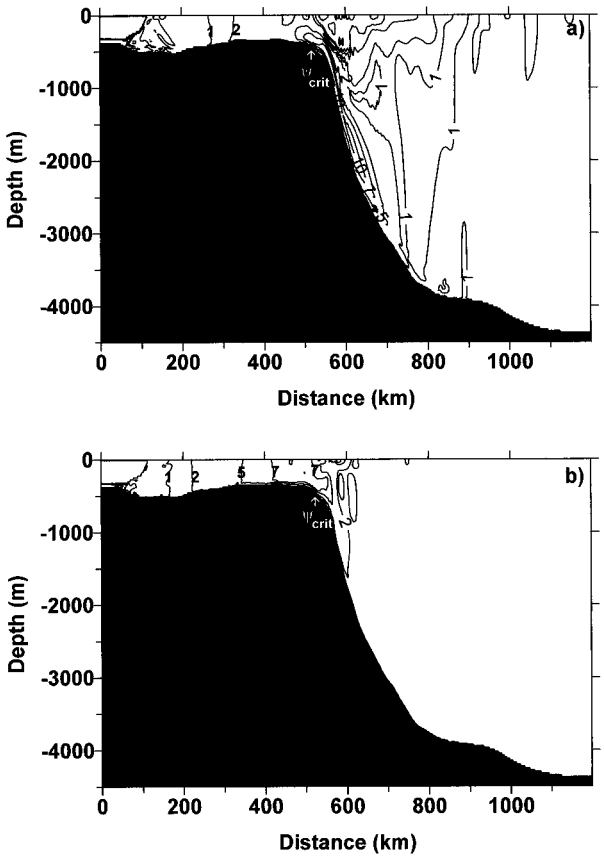

FIG. 6. The major axes of the tidal ellipses of the depth-dependent velocities (cm s^{-1}) from simulations with the critical latitude in the domain and a stratified ocean from (a) the original version of POM and (b) the modified version of POM.

the BPG term in the baroclinic pressure gradient subroutine (BAROPG); in other words, ρ_{MEAN} was not removed from ρ before the calculation.

Other modifications were made to POM to increase the accuracy of the density calculation. These modifications include using double precision for all variables, using a mean density (ρ_o) based on the potential temperature and salinity biases at the ocean surface, normalizing the density by ρ_o instead of 1000, and using 1449.2 instead of 1449.1 in the calculation of the speed of sound in the density pressure corrections. These modifications effectively change the set of density calculations from (4)–(8) to

$$\rho = \frac{\rho_{\theta,S}}{\rho_o} - 1. \qquad \rho_o = \rho_{\theta,S}(\theta_{\text{Bias}}, S_{\text{Bias}}).$$

$$c = 1449.2 + 0.00821p + 4.55\theta - 0.45\theta^2 + 1.34(S - 35). \tag{23}$$

These corrections are, however, minor compared with removing the η-dependent error in the BPG calculation (i.e., removing the pressure contribution to the density).

For these studies of tides in the southern Weddell Sea, POM was also modified to accommodate the existence of an ice shelf. This is unnecessary for most other locations. A term was added for friction at the ice shelf base as a surface stress for the ice shelf portion of the domain. In addition, the pressure head of the ice shelf was accounted for in pressure calculations at depth, with σ scaled by the water column thickness (depth from seabed to ice base) instead of the bottom depth. The ice shelf was assumed to float freely.

4. Test of model amendments

Having made the previously described modifications to POM, the Weddell Sea cases were re-run, for both a homogeneous and a realistically stratified ocean. In the homogeneous case (Fig. 5a), the velocity field now appears well behaved over the slope when compared with the uncorrected model run (Fig. 2a). Note that Fig. 2a shows the effect of diffusion of momentum upwards from the bottom-intensified oscillation due to $\text{BPG}_{\text{error}}$. In a stratified case with the uncorrected POM code, the vertical variation of V is more intensified towards the seabed (see Fig. 6a) because the model-generated vertical viscosity K_M is very much smaller than in the homogeneous case. In a stratified case, depth-dependent velocity structure in the corrected model run (Fig. 5b) is constrained to the region where linear wave theory predicts internal tide generation, over the upper slope. The large benthic oscillation that was evident in the M_2 tidal ellipse major axes with the uncorrected model (Fig. 6a) was not present when POM was modified (Fig. 6b). Internal tides also existed in the unmodified version of POM with stratification, but were obscured by the signal due to $\text{BPG}_{\text{error}}$ (Fig. 6a). Some tidal observations have been made in this region and are fully described in Robertson et al. (1998) and Robertson (1999). The major axes of the tidal ellipses predicted by the modified version of POM agree within the approximate measurement uncertainty (2 cm s^{-1}) for 15 of the 19 observations (Table 1). This agreement is encouraging, especially since many of the observations are not exactly along the transect and often have different water depths than at their location mapped onto the transect line. A more complete discussion of the observational data is given in another study (Robertson 2001a,b).

It was concluded that these modifications to the calculation of density in POM eliminated a small but sometimes significant error in the baroclinic pressure gradient term. Removing this error was found to be crucial to obtaining a satisfactory model solution for baroclinic tide generation in the vicinity of the tidal constituent's critical latitude. It was not investigated whether this error is primarily a problem only when forcing is purely sinusoidal at a single frequency near f; it is possible that additional energy sources prevent the resonant growth of the inertial mode. However, no known problems were introduced to POM by these proposed solutions, and it is therefore recommended that the so-

TABLE 1. Comparison between POM and Robertson, Padman, and Edbert (1998) predictions and the observations for the major axis of the tidal ellipses (cm s^{-1}) at the observation locations. The location and water depth are given for each of the observations along with the principal author and year of the reference. The differences are shown in parentheses. A dash indicates a difference less than the observational uncertainty.

Location	Reference	On or off transect	Water depth (m)			M_2 major axis for tidal velocity ellipse	
			Observation	Model	Instrument	Observation	POM
75°1′S, 31°46′W	Woodgate et al. (1998)	Off	610	362	257	5.7	5.3 (−)[c]
				(601)[b]	378	6.3	7.3 (−)
					484	6.4	6.2 (−)
					590	5.3	2.5 (−3)
75°2′S, 33°33′W	Woodgate et al. (1998)	Off	574	365	191	7.1	7.0 (−)
				(582)[b]	342	6.3	7.2 (−)
					448	5.5	5.2 (−)
					554	3.3	0.9 (−2)
74°40′S, 33°56′W	Middleton et al. (1982)[a]	Off	475	379	375	6.8	7.2 (−)
					450	4.5	3.6 (−)
74°26′S, 39°24′W	Middleton et al. (1982)[a]	On	475	483	375	6.8	7.6 (−)
					450	3.4	2.5 (−)
74°24′S, 39°6′W	Middleton et al. (1982)[a]	On	465	507	400	5.0	7.4 (+2)
					450	2.6	1.2 (−)
74°23′S, 37°39′W	Foldvik et al. (1990)	Off	475	518	450	2.2	1.3 (−)
74°8′S, 39°19′W	Foldvik et al. (1990)	On	650	828	627	3.0	0.3 (−3)
74°6′S, 39°22′W	Middleton et al. (1982)[a]	On	720	868	620	2.9	2.2 (−)
73°43′S, 38°36′W	Middleton et al. (1982)[a]	On	1915	1906	1815	1.3	1.7 (−)
					1890	0.9	1.5 (−)

[a] Foldvik et al. (1990) is a more useful reference for these observations.
[b] Depth for the altered position.
[c] Differences shown in parentheses with dash for difference indicating the value agreed within the uncertainty range.

lutions be implemented even when the model is applied to regions well removed from critical latitude effects.

Acknowledgments. This study was supported by NSF Contract OPP-9896041. We would like to thank Drs. Andrew Bennett, John Allen, and Ricardo Matano for their help in locating the problem in POM.

REFERENCES

Blumberg, A. F., and G. L. Mellor, 1987: A description of a three-dimensional coastal ocean circulation model. *Three-Dimensional Coastal Ocean Models*, N. Heaps, Ed., Vol. 4, *Coastal and Estuarine Sciences,* Amer. Geophys. Union, 1–16.

Chen, C., and R. C. Beardsley, 1998: Tidal mixing and cross-frontal particle exchange over a finite amplitude asymmetric bank: A model study of Georges Bank. *J. Mar. Res.,* **56,** 1163–1201.

Foldvik, A., J. H. Middleton, and T. D. Foster, 1990: The tides of the southern Weddell Sea. *Deep-Sea Res.,* **37,** 1345–1362.

Foreman, M. G. G., 1978: Manual for tidal current analysis and prediction. Pacific Marine Science Rep. 78-6, Institute of Ocean Sciences, Patricia Bay, Sidney, BC, Canada, 70 pp.

Furevik, T., and A. Foldvik, 1996: Stability at M_2 critical latitude in the Barents Sea. *J. Geophys. Res.,* **101,** 8823–8837.

Holloway, P. E., 1996: A numerical model of internal tides with application to the Australian northwest shelf. *J. Phys. Oceanogr.,* **26,** 21–37.

Kleim, N., and J. D. Pietrzak, 1999: On the pressure gradient error in sigma coordinate ocean models: A comparison with a laboratory experiment. *J. Geophys. Res.,* **104,** 29 781–29 799.

Kundu, P., 1990: *Fluid Mechanics.* Academic Press, 668 pp.

Mellor, G. L., 1991: An equation of state for numerical modeling of oceans and estuaries. *J. Atmos. Oceanic Technol.,* **8,** 609–611.

——, 1998: User's guide for a three-dimensional, primitive equation, numerical ocean model. Report of the Atmospheric and Ocean Sciences Program, Princeton University, Princeton, NJ, 41 pp. [Available online at http://www.aos.princeton.edu/WWWPUBLIC/htdocs.pom].

——, T. Ezer, and L.-Y. Oey, 1994: The pressure gradient conundrum of sigma coordinate models. *J. Atmos. Oceanic Technol.,* **11,** 1126–1134.

——, L.-Y. Oey, and T. Ezer, 1998: Sigma coordinate pressure gradient errors and the seamount problem. *J. Atmos. Oceanic Technol.,* **15,** 1122–1131.

Middleton, J. H., and T. Denniss, 1993: The propagation of tides near the critical latitude. *Geophys. Astrophys. Fluid Dyn.,* **68,** 1–13.

——, and T. D. Foster, 1977: Tidal currents in the central Weddell Sea. *Deep-Sea Res.,* **24,** 1195–1202.

——, ——, and A. Foldvik, 1982: Low-frequency currents and continental shelf waves in the southern Weddell Sea. *J. Phys. Oceanogr.,* **12,** 618–634.

Robertson, R., 1999: Mixing and heat flux mechanisms in the upper ocean in the Weddell Sea. Ph.D. thesis, Oregon State University, 173 pp.

——, 2001a: Internal tides and baroclinicity in the southern Weddell Sea. Part I: Model description. *J. Geophys. Res.,* in press.

——, 2001b: Internal tides and baroclinicity in the southern Weddell Sea. Part II: Effects of the critical latitude and stratification. *J. Geophys. Res.,* in press.

—— L. Padman, and G. D. Egbert, 1998: Tides in the Weddell Sea. *Ocean, Ice and Atmosphere: Interactions at the Antarctic Continental Margin.* Antarctic Research Series, S. S. Jacobs and R. F. Weiss, Eds., Vol. 75, Amer. Geophys. Union, 341–369.

Woodgate, R. A., M. Schröder, and S. Østerhus, 1998: Moorings from the Filchner Trough and the Ronne Ice Shelf Front: Preliminary results, H. Oerter, Ed., Filchner-Ronne Ice Shelf Program, Alfred-Wegener Institute Rep. 12, 85–90.